Hindawi
Advances in Civil Engineering
Volume 2020, Article ID 6198594, 17 pages
https://doi.org/10.1155/2020/6198594

Research Article

Seismic Performance Assessment of Reinforced Concrete Frame-Shear Wall Structures in Hydropower Plants Based on Material Damage

Changzheng Shi,[1] Lei Hu,[2] He-Gao Wu ,[1] Qi-Ling Zhang ,[2] and Kai Su[1]

[1]*State Key Laboratory of Water Resources and Hydropower Engineering Science, Wuhan University, Wuhan 430072, China*
[2]*Changjiang River Scientific Research Institute, Wuhan 430010, China*

Correspondence should be addressed to He-Gao Wu; hgwu@whu.edu.cn

Received 11 October 2019; Revised 11 June 2020; Accepted 27 August 2020; Published 10 September 2020

Academic Editor: Zhongguo John Ma

For the reinforced concrete frame-shear wall (RCF-SW) structures in hydropower plants (HPs), the tensile cracking and compressive crushing of the reinforced concrete (RC) members are considered as the main potential damage. This paper presents a methodology to assess the seismic performance of RCF-SW structures. In this methodology, a concrete damage plasticity model is employed to simulate the reinforced concrete, and the structural seismic responses are investigated through nonlinear incremental dynamic analysis (IDA). Several engineering demand parameters (EDPs) based on the material damage are proposed to identify the structural engineering limit states and damage states at the member level. The case of x HP is provided as an example to illustrate the methodology and discuss the probable nonlinear response and structural damage state. The concrete damage evolution, reinforcement stresses, and drift ratios of the RCF-SW structure are presented, and the engineering limit states and structural damage states are identified. In comparison with the drift ratio index, the EDPs based on material damage are more suitable for identifying the damage state of the RCF-SW structure, whose damage is controlled by the damage of the RC members.

1. Introduction

In recent years, performance-based seismic design (PBSD) has emerged as one of the most important advances in seismic engineering [1–3]. In this methodology, the structural criteria are expressed in terms of achieving a performance objective, which is the coupling of an expected structural damage level and an expected earthquake severity level. The performance levels describe the structural damage states and consequential losses which may be incurred in terms of casualties, property, and operational capacity [4–6].

In the design of hydraulic structures, the traditional seismic design focuses on protecting human life by preventing local or global collapse at a specific earthquake level. In recent years, engineering communities have been aware of the importance of property and other economic losses caused by more frequent earthquakes. Thus, PBSD has become useful for the seismic evaluation of hydraulic structures, such as dams and water intake towers. The seismic performance assessment methods and nonlinear dynamic analysis methods of dams are well established [7–13]. However, few experimental and analytical studies have investigated the seismic performance of hydropower plants (HPs). In fact, the investigation of damage incurred by hydropower stations during the Wenchuan earthquake indicates that HPs are damaged more heavily than dams [14].

Generally, an HP can be divided into three parts: the main powerhouse, erection bay, and auxiliary powerhouse. The main powerhouse and auxiliary powerhouse house the turbine generator units and auxiliary electrical and mechanical equipment (see Figure 1). The safety of HPs ensures the power generation and staff safety. Thus, the seismic performance of HPs should be taken seriously. Typically, HPs are divided into substructures and superstructures

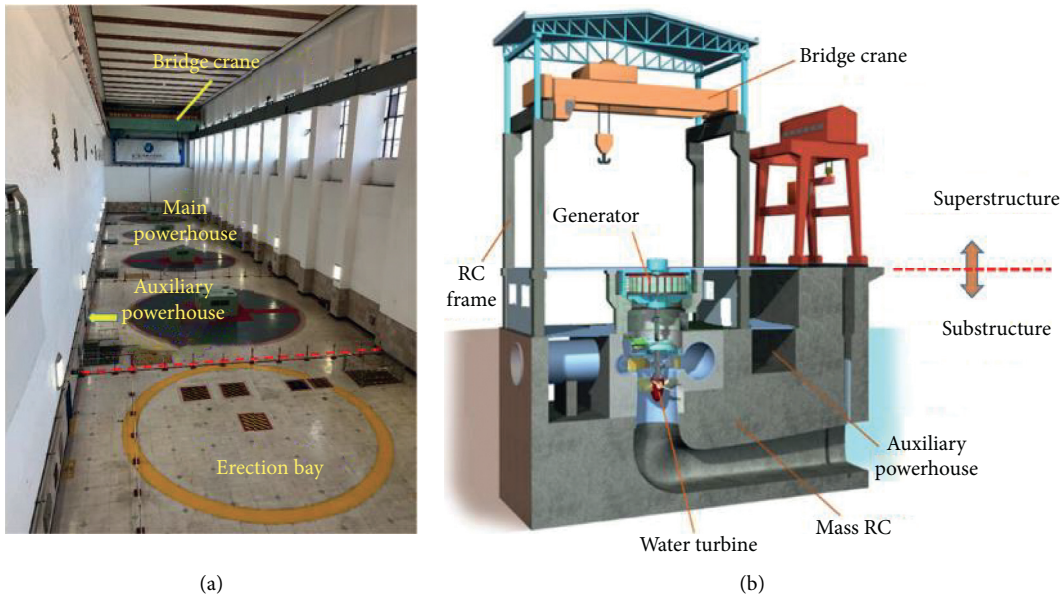

Figure 1: Basic components of an HP: (a) typical layout and (b) typical profile of the main powerhouse.

according to their distinctive structural features (see Figure 1). The substructures are mass concrete structures, wherein turbine generator units are set, while the superstructures are composed of reinforced concrete (RC) frames and shear walls. A bridge crane travels along the tracks supported by the RC frame in the main powerhouse and erection bay. The crane is used for the installation or maintenance of the generator units and other types of equipment. Because of the sharp distinctions in mass and stiffness between the substructure and the superstructure, the superstructures are vulnerable during earthquakes [15, 16]. For example, the superstructure of the CaoPo HP was severely damaged during the Wenchuan earthquake. As shown in Figure 2, several cracks appeared, and the joints between the endwalls and the sidewalls opened. Though the HP did not collapse in the earthquake, the repair of structures and equipment was time-consuming and expensive. Moreover, a long-lasting outage led to a great financial loss. Therefore, the need to shift the focus of HP seismic design from strength to performance has been highlighted.

In the PBSD process, the identification and assessment of the structural performance are critical tasks. The PBSD implementation requires the prediction of structural demands and capacities and the identification and quantification of the damage state associated with different performance levels. In traditional design, the seismic performance of HPs is assessed on the basis of simple stress or section-force checks, which are obtained by linear earthquake analysis [17, 18]. However, it is difficult to use linear analysis to identify the structural performance levels when the structural responses change from the elastic state to a failure limit state. Incremental dynamic analysis (IDA) is a well-known method of quantitatively estimating the structural limit states. In IDA, the intensity of the ground motion applied to the structure is increased incrementally until the limit states are reached [19]. This method has been widely applied to assess the collapse capacity of buildings and bridges [20–22].

In an IDA study, the results are presented in terms of earthquake intensity-damage measure curves. The earthquake intensity is defined by the intensity measure (IM). The damage is defined as the degradation of structural bearing capacity and durability. The PGA and spectral accelerations are often used as the IM. Generally, to evaluate the damage in a structure, the damage measures (DMs) or engineering demand parameters (EDPs) are used. Commonly used DMs or EDPs include stress, strain, deformation, reactions, crack length and stiffness, and energy dissipations [4, 8, 23–27]. Previous experimental studies indicate that none of these DMs consistently predict observed damage limit state [28–30]. Thus, the quantitative relationships between the EDPs and the performance levels and a clear definition of limit states are still under investigation. For RC frame structures, global responses of the structure are evaluated in terms of peak roof drift ratios, peak interstory drift ratios, interstory drift ratios envelopes, normalized roof displacements relative to the motion of the center of gravity of the roof, and dissipated energy. Local responses assessed include moment-curvature or moment-rotation response in beams and columns as well as the hysteretic energy dissipated at selected sections of the structure [31]. In the structural damage assessment of RC frame structures, the story drift ratio is well known and frequently utilized. FEMA-273 [4], FEMA-356 [5], GB 50011-2010 [32], Smith [33], and Xin et al. [34] provide various deformation limits or drift limits for RC frames and shear walls to define the structural performance levels. However, Ghobarah et al. [35] and Hancock et al. [36] showed that story drift ratio did not account for the influence of cumulative damage due to repeated inelastic deformation and was properly considered for the damage caused by extreme displacement. Belejo et al.

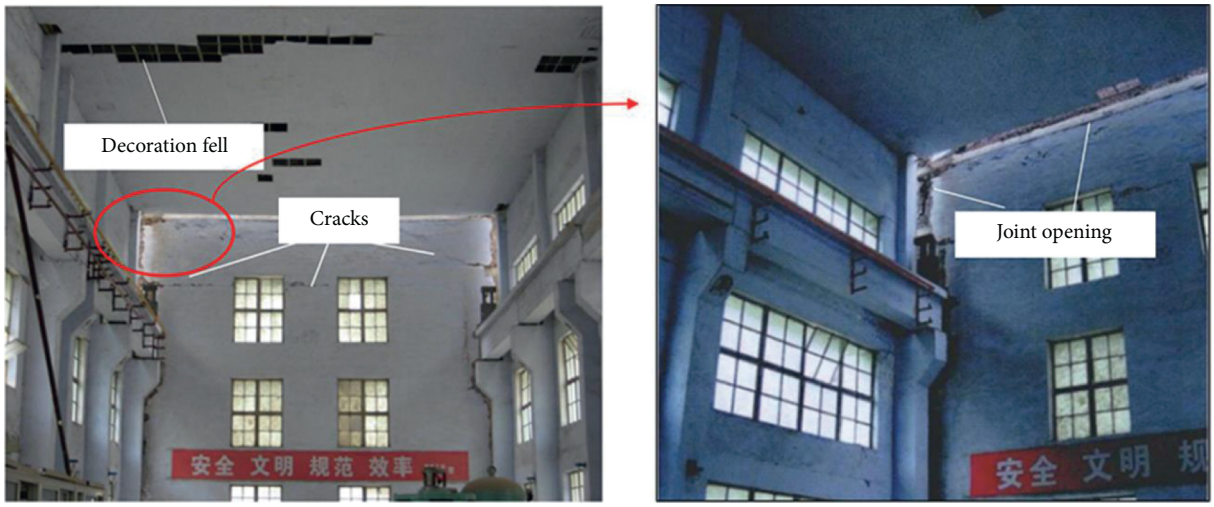

Figure 2: Damage caused by Wenchuan earthquake in CaoPo HP.

[31] and Chandramohan et al. [37] concluded that the drift ratio index had a lack of capability to capture the effect of degrading energy capacity and in-cycle strength degradation. Moreover, although the story drift is suitable for interpreting the overall structural damage state, it cannot predict the progressive damage incurred by the RC members. However, the damage incurred by an RC structure is generally related to the failure of component members. Particularly, in the HP, the RC columns and beams are much stronger than those of ordinary buildings. Thus, the prediction of damage at element level is more important.

Generally, the failure of RC members is mainly caused by the crushing of concrete, which begins with the spalling of the concrete cover and ends with the crushing of the concrete core. Because finite element analysis (FEA) tools and computer technology have been rapidly evolving in recent years, given the advances in computational methods for nonlinear structural analysis, it has become feasible and more convenient to use damage constitutive models to track the process of damage occurrence in RC structures [38–40]. The mechanical properties of concrete are controlled by the generation and growth of microcracks. The microcracks in concrete will expand, grow, and converge under various loads, and then the macrocracks form, leading to strength degradation or even material failure. In the damage constitutive model, damage variables are introduced to characterize the effect of microcracks on macromechanical properties of concrete. The damage variables of concrete are usually defined as the degradation of elastic modulus. According to tensile and compression tests of concrete, semiempirical relationships between damage variables and macromechanical parameters, such as strain, can be obtained. The applications of the damage constitutive model exhibit computational efficiency and suitability to the simulation of the initiation and propagation of concrete material deterioration against strong earthquakes, and the calculated tensile and compressive damage variables reveal the essential reasons for the occurrence of structural damage at the material level. Therefore, in recent years, various EDPs and DMs based on the material damage have been proposed [41–43]. Most of these DMs consider the damage of the most critical fibers of concrete and reinforcement as representative damage for each section, and the structural damage indices are typically defined as the function of the maximum material damage values of concrete and reinforcement. However, the maximum material damage cannot demonstrate the structural damage extent and progress at all times. For example, the large tensile damage and the large damage in the local area cannot predict the failure of an RC member. Therefore, the structural damage indices based on material damage require further investigation.

In this study, to assess the damage incurred by RC frame-shear wall (RCF-SW) structures in HPs, an IDA investigation was conducted. The plastic-damage model for concrete proposed by Lee and Fenves [44] was used to carry out nonlinear analysis and determine the material damage propagation in RCF-SW structures. Several EDPs based on material damage have been proposed to predict the structural damage states of the RCF-SW at the member level. These EDPs are linked to engineering limit states such as the cracking, spalling, and crushing of concrete, and the relationships between the engineering limit state and the structural damage state have been established. Finally, the structural damage states have been assessed by the EDPs.

2. Nonlinear FEA

Using the commercial FEA software ABAQUS [44], nonlinear time-history analyses were performed to predict the performance of the HPs. The main issues that significantly influence the seismic responses of HPs are the constitutive behavior relationships employed for concrete and steel.

2.1. Plastic-Damage Model of Concrete. The plastic-damage model of concrete proposed by Lee and Fenves [45] was employed to simulate the nonlinear constitutive behavior of concrete, and this model is available in ABAQUS. The basic

notion of the plastic-damage model is the coupling of isotropic damaged elasticity with isotropic tensile and compressive plasticity to describe the irreversible damage incurred during the loading process. In this model, the stress-strain relationship of concrete is expressed as follows:

$$\boldsymbol{\sigma} = (1-d)\mathbf{D}_0^{\mathbf{el}} : \left(\boldsymbol{\varepsilon} - \boldsymbol{\varepsilon}^{\mathbf{pl}}\right) = \mathbf{D}^{\mathbf{el}} : \left(\boldsymbol{\varepsilon} - \boldsymbol{\varepsilon}^{\mathbf{pl}}\right), \quad (1)$$

where ε is the total strain; $\varepsilon^{\mathbf{pl}}$ is plastic strain; $\mathbf{D}_0^{\mathbf{el}}$ is the initial elastic stiffness of the undamaged concrete; $\mathbf{D}^{\mathbf{el}}$ equaling $(1-d)\mathbf{D}_0^{\mathbf{el}}$ is the elastic stiffness of the damaged concrete; d is the damage variable reflecting the degradation of stiffness. With the accumulation of concrete damage, the value of d varies from 0 (no damage) to 1 (fully damaged).

The definition of the scalar degradation variable d must be consistent with the uniaxial monotonic responses (uniaxial damage variable in compression d_c and uniaxial damage variable in tension d_t) and should also capture the complexity associated with the degradation mechanisms under cyclic loading. With regard to the general multiaxial stress conditions, the model makes the following assumption:

$$\begin{aligned} (1-d) &= \left(1 - s_t d_c\right)\left(1 - s_c d_t\right), \quad 0 \le s_t, s_c \le 1, \\ &\begin{cases} s_t = 1 - w_t r\left(\hat{\bar{\sigma}}\right), & 0 \le w_t \le 1, \\ s_c = 1 - w_c\left(1 - r\left(\hat{\bar{\sigma}}\right)\right), & 0 \le w_c \le 1, \end{cases} \end{aligned} \quad (2)$$

where variables s_t and s_c represent the stiffness recovery effect as a function of stress state $r(\sigma)$. $r(\sigma)$ is a stress weight factor equal to one if all principal stresses are positive or equal to zero if all principal stresses are negative. The parameters w_t and w_c control the recovery degree of the tensile stiffness and compressive stiffness. In most quasibrittle materials, including concrete, it has been observed experimentally that the compressive stiffness is recovered upon crack closure as the load shifts from tension to compression. However, once crushing microcracks have developed, the tensile stiffness is not recovered as the load shifts from compression to tension. This behavior is used by default in ABAQUS, as shown in Figure 3.

2.2. Model of Reinforcing Bars. The bilinear kinematic hardening constitutive model (see Figure 4(a)) was recommended for the reinforcing bars [46]. The hardening modulus was determined according to the stress-strain relationship of the steel material shown in Figure 4(b). By drawing a straight line between the yield strength point (f_y; ε_y) and the ultimate strength point ($k_4 f_y$; $k_2 \varepsilon_y$), it can be seen that the slope of the straight line is the equivalent hardening modulus of the steel material.

2.3. Comparison to Test Data. To validate the nonlinear FE model, predictions using the model are compared to cyclic quasistatic test on reinforced concrete columns conducted by Du [43]. The predictions of the tested column specimen are shown in Figure 5. It can be seen that the overall behavior is well predicted as evidenced by the loading and unloading branches. The largest tensile damage concentration

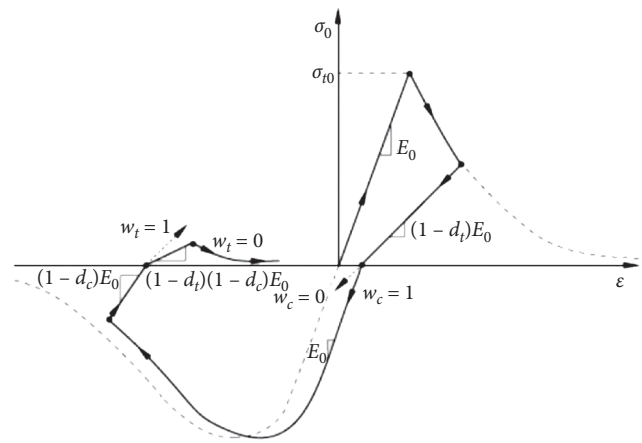

Figure 3: Uniaxial load cycle assuming default values for the stiffness recovery factors ($w_t = 0$ and $w_c = 1$) [44].

predicted was located in the plastic hinge region at the column base. As can be seen from the figure, the predicted damage in tension and compression is in a good agreement with the concrete cracks and spalling shown in the test. The excellent prediction reflects that the model does a good job of taking into account the concrete crack closure mechanism, and the local behavior of the reinforced concrete element, such as cracking of concrete, progressive spalling of the concrete cover, and yielding of the reinforcement, can be well predicted.

3. IDA

3.1. Earthquake Ground Motions and IM. In an IDA study, a series of earthquake ground motions is applied to the structure. By increasing the shaking intensity, the structural initial elastic state shifts to an inelastic state and finally to a collapsed state. Thus, the seismic performance and progressive limit states of the structure can be identified up to its collapse. The most frequently selected IMs are the PGA, PGV, and 5%-damped spectral acceleration at the fundamental period of the structure $S_a(T_1, 5\%)$. Alembagheri and Ghaemian [9] reported that using $S_a(T_1, 5\%)$ can obtain less scattered results. Thus, in this study, $S_a(T_1, 5\%)$ was selected as the IM.

3.2. EDPs. Considering the huge loads and importance of HPs, the size of the RC members and the quantity of reinforcement are frequently large. Thus, the collapse of the entire HPs hardly ever occurs during earthquakes. Related studies [15, 16] have shown that the cracking and crushing of the RC columns and walls, which is induced by cyclic shaking and flexural loads, is the main damage mode of HPs.

Kunnath et al. [28] conducted a comprehensive experimental study to investigate cumulative damage in RC columns under cyclic loads and typical earthquakes. Du [43] conducted pseudostatic tests on RC columns, and the structural damage process and the failure modes were presented in detail. A set of 21 RC column specimens test at the University of Sherbrooke under cyclic flexure represented the structural damage evolution of RC columns [47]. These experimental studies correlated visually observed

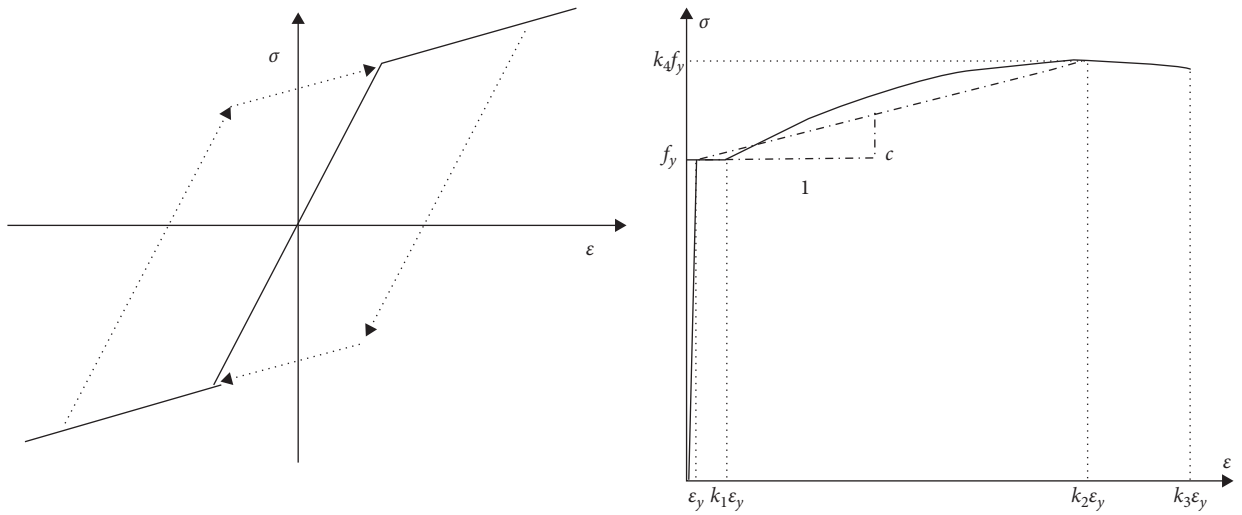

(a) (b)

Figure 4: Constitutive model of steel bar. (a) Bilinear kinematic hardening constitutive model. (b) Response of bars under uniaxial tensile load [45].

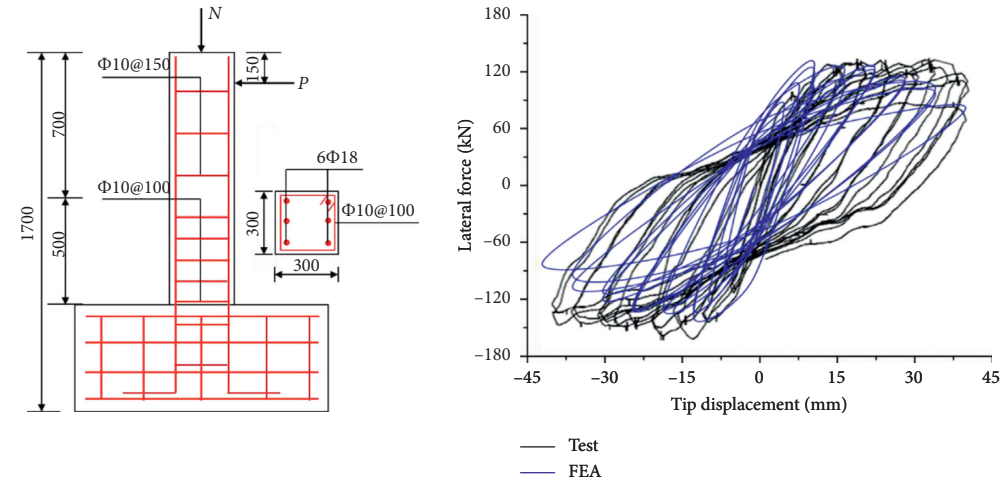

(a) (b)

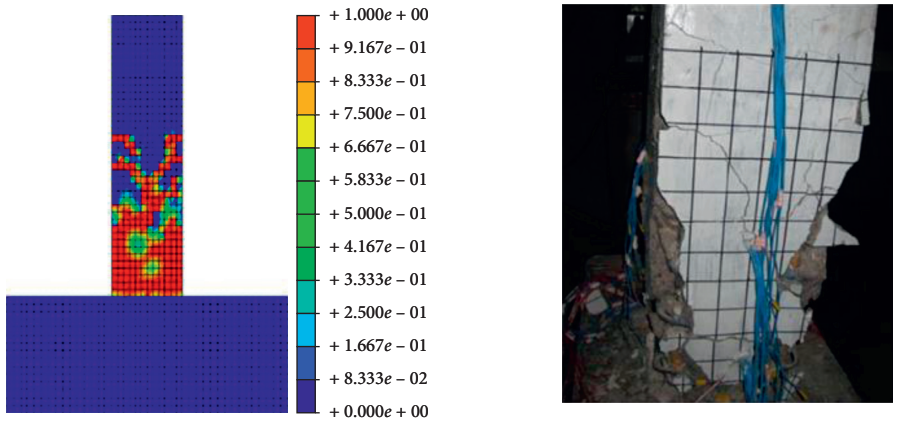

(c) (d)

Figure 5: Continued.

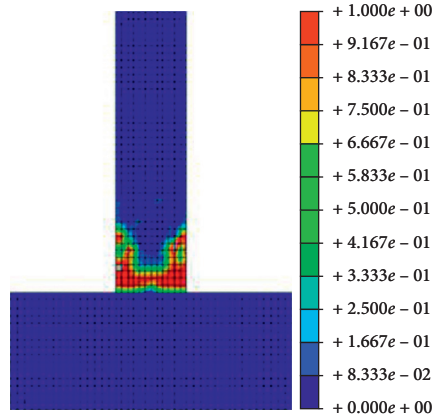

(e)

Figure 5: Prediction of the behavior of column tested by Du [43]. (a) Column specimen. (b) Force-displacement response. (c) Damage in tension prediction. (d) Damage in plastic hinge zone at the end of the test. (e) Damage in compression prediction.

damage during testing with damage limit states. The correlations of damage limit states with visual observations are summarized in Table 1. As is shown in the table, the critical task of the damage state identification is tracking the cracking and spalling process of concrete and the buckling process of bars.

Based on the test results, the material damage zone distribution diagram of RC columns can be simplified to the shadows shown in Figure 6. Usually, the tensile and compressive damage originate at the column base and develop along the section height and column height directions. Under earthquake excitation, tensile damage may originate at one side of the column, and d is defined as the tensile damage evolution depth at the column base. However, tensile damage develops quickly, occurs at the other side of the column, and extends over the entire column base. The tensile damage reduces slowly above the column base over the height of the column. Additionally, the cracks cutting through the sections appear in sequence over the height of the column. Then, a plastic hinge zone starts to form near the column base [43, 47]. Once the reinforcement yields and the plastic hinge zone forms, the displacement of the column increases more rapidly as the loads increase. Therefore, the formation of the plastic hinge is a limit state for the RC columns.

Generally, the tensile damage incurred by the RC columns under flexural loads will be more severe than the compressive damage. However, the collapse of the RC columns is related to the severe crushing rather than cracking. As shown in Figure 6, the compressive damage decreases rapidly from the concrete cover to the concrete core owing to the reinforcement. The spalling of the concrete cover occurs first, and then the concrete core begins to crush as the compressive damage evolves [43, 47]. The extent of spalling and crushing of the concrete reveals the damage state incurred by the RC frame. The damage distribution of the wall in the thickness direction is similar to that of the column. For the walls, h represents the wall thickness.

Cardona et al. [48] conducted a series of experimental tests and numerical calculations with RC columns and reported the relationship between the concrete material damage and engineering limit state, such as cracking, spalling, and crushing. Based on related investigation on the damage incurred by RC columns, in this study, several EDPs are proposed based on material damage to evaluate the damage state of the RC members. These EDPs include the following:

(i) d/h, the ration of tensile damage (≥ 0.7) evolution depth d at the column base section to section height h.

(ii) $D_{\text{c-cover}}$, the average compressive damage of concrete cover at the column base section.

(iii) $D_{\text{c-core}}$, the average compressive damage of concrete core at the column base section.

(iv) σ_s, the maximum value of reinforcement stress.

For normal strength concrete, macroscopic cracks appear when the tensile damage value reaches approximately 0.6-0.7. Therefore, the tensile damage evolution index d/h is obtained according to the profile of tensile damage values larger than 0.7 to describe the crack propagation lengthening at the column base. When $d/h = 1$, the crack cutting through the column base appears, and the plastic hinge initiates. The spalling of the concrete cover begins at $D_{\text{c-cover}} = 0.1$, and the crushing of the concrete core begins at $D_{\text{c-core}} = 0.1$. When $D_{\text{c-cover}}$ is equal to 0.5, obvious spalling of concrete cover occurs. When $D_{\text{c-cover}}$ is equal to 0.8, the concrete cover spalling becomes severe. Moreover, the crushing of the concrete core becomes severe when $D_{\text{c-core}}$ is equal to 0.5 [48].

3.3. Damage States. This current study linked EDPs based on the material damage to the engineering limit states such as concrete cracking, concrete cover spalling, and concrete core crushing (Table 2). Then, in accordance with the engineering limit states, this current study divided the damage states into four levels: negligible, light, moderate, and severe.

At the first damage level, most of the concrete is still in the elastic stage. Because the tensile strength is far less than

Table 1: Correlation of damage limit states with visual observation [28, 43, 47].

Damage state	Description	Visual observation
None	No visible damage, either cosmetic or structural	No visible cracks
Insignificant	Damage requires no more than cosmetic repair. No structural repairs are necessary	Hairline cracks Minor spalling
Moderate	Repairable structural damage has occurred. The existing element can be repaired essentially in place, without substantial demolition or replacement of elements	Excessive spalling Exposed reinforcement No buckling of bars
Heavy	Damage is so extensive that repair of elements either is not feasible or requires major demolition or replacement	Buckling/fracture of bars

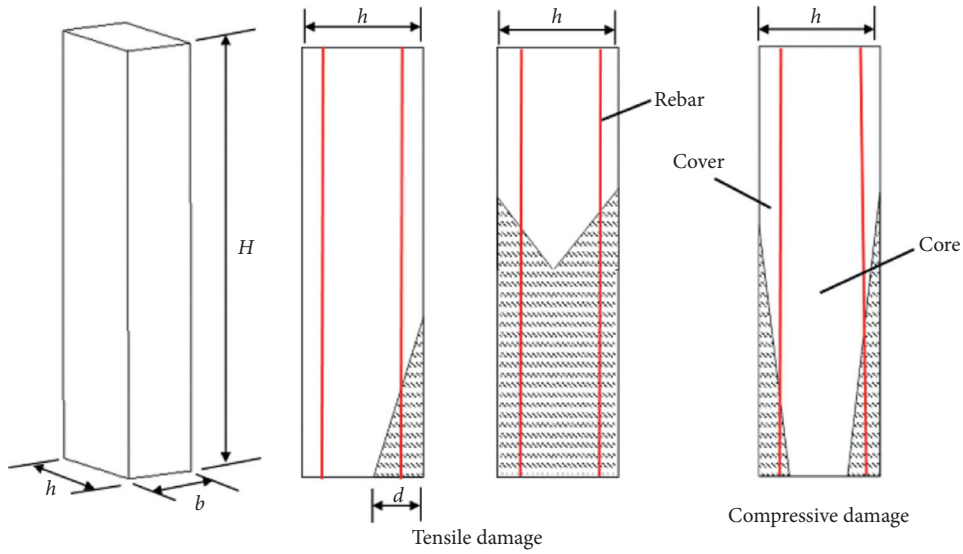

Figure 6: Material damage distribution in column under flexural loads [43].

Table 2: Relationship between damage states, engineering limit states, and material damage.

Damage state	Engineering limit state	d/h	$D_{c-cover}$	D_{c-core}	σ_s
Negligible	Concrete cover cracking onset	0.1	≈0	≈0	
Light	Concrete cover spalling onset		0.1		
	Plastic hinge initiating	1			
Moderate	Concrete cover important spalling		0.5		
	Concrete core crushing onset			0.1	
	Reinforcement yielding				σ_y
Severe	Concrete cover severe spalling		0.8		
	Concrete core important crushing			0.5	

Note. σ_y is the yield strength of reinforcement.

the compressive strength, cracks may appear at the local zones, such as the ends or surface of the RC members. However, these small cracks do not exert significant influence on the bearing behavior of the members. Therefore, at this stage, the damage of the entire structure is negligible.

At the second damage level, the stiffness of the structure is reduced owing to the rapid evolution of concrete tensile damage. The cracks at the column base penetrate the entire section, and new cracks appear continuously along the height of the members. Concurrently, the reinforcement stresses increase rapidly. At this stage, the plastic hinge begins to form at the column base. While the concrete compressive damage in the RC member is still at a low level, only the spalling of the concrete cover initiates at local zones. At this stage, the structure incurs only light damage.

At the third damage level, the stiffness of the structure is reduced owing to the evolution of concrete compressive damage. The compressive damage in concrete cover has gone through a rapid development stage and enters into a smooth development stage. The spalling of concrete cover becomes important because serious spalling of concrete cover leads to the exposure of reinforcement. With the

increase of the compressive damage zones and extent of compressive damage, the spalling of the concrete cover and crushing of the concrete core become obvious, and the reinforcement yields concurrently. The degeneration of compressive capacity exerts a significant influence on the structural bearing capacity. Thus, at this stage, the damage incurred by the structure is regarded as moderate.

At the last damage level, the concrete compressive damage accumulates, and the spalling of the concrete cover and the crushing of the concrete core become severe. The plastic hinge enters into the failure stage, and the stiffness of the structure becomes low and results in a significant decrease of the structural bearing capacity. At this damage state, the structure tends to collapse.

4. FEA of Jx HP

The Jx hydropower station is still in the design process. The installed generation capacity of the plant is 560 MW and is provided by four water-turbine generator sets. The HP is located at the toe of the concrete gravity dam. The site of the hydropower station is in a seismically active region. The PGA with a probability of exceedance 2% per 50 years is 0.331 g, and that with a probability of exceedance of 1% per 100 years is 0.498 g.

A finite element (FE) model was developed as shown in Figure 7. The model consists of the HP and foundation. The ABAQUS software was used to conduct the analysis. The concrete structure and foundation were meshed using C3D8 solid elements, the steel structure was meshed using S4 shell elements, and the roof grid was meshed using T3D2 truss elements. A viscous-spring artificial boundary was used to simulate the effect of radiation damping, and the spring-dashpot system was modeled using spring elements and dashpot elements. Considering the material nonlinearity of the RC structure, the steel bars were also simulated. In this study, an embedded discrete reinforcement model was employed and a 2-node truss element was used. The reinforcement elements were assumed to be fully embedded in the solid concrete element without sliding. The FE model contains 329,667 elements and 347,956 nodes.

The seismic analysis focuses on the superstructure of the powerhouse; therefore, only the steel bars in the walls, columns, and floors above the generator floor were included in the model. The mass concrete structure under the generator floor has a good seismic performance, and cracks are typically induced by internal water pressure. However, the local cracks in the mass concrete cannot significantly influence the seismic performance of the superstructure. Thus, the reinforcement in the concrete mass under the generator floor was not simulated, and the material nonlinearity of the mass concrete was ignored. A previous study [49] has reported that this assumption has little effect on the dynamic characteristics of the superstructure and can reduce the required computational cost.

The plastic-damage model was used to describe the damage caused by the yielding of the concrete, and the Mazars damage model was used to calculate the tensile and compressive damage values according to the stress and strain states of the concrete. A bilinear kinematic hardening model was employed for steel. A linear elastic constitutive model was used for the foundation rock to reduce the computational cost. The material properties used in the simulation are listed in Table 3. The uniaxial stress-strain and damage-strain curves in tension and compression of concrete are shown in Figure 8. According to GB 50010-2010 [46], the ultimate strain of the bars is taken as 0.05, so the yield strain $\varepsilon_y = 0.002$ and $k_2 = 25$.

In this study, the ten earthquake ground motions listed in Table 4 were selected for IDA investigation. These records are downloaded from Pacific Earthquake Engineering Research Center (PEER) Ground Motion Database (https://peer.berkeley.edu/peer-strong-ground-motion-databases). The 5%-damped acceleration response spectrum curves of all earthquake records are shown in Figure 9. The spectral accelerations at the fundamental period of the structure 0.62 s (denoted as S_a) are also listed in Table 4. In the IDA, for each record, the IM $S_a(T_1, 5\%)$ was set to increase from 0.05 g to 1.0 g with an interval of 0.05 g or 1.0 g, and for each earthquake intensity, a nonlinear analysis was done. If the original record is denoted as $a(t)$, the amplitude modulation record used in the analysis $a_\lambda(t) = \lambda a(t)$. Here, the amplitude modulation factor λ is equal to $S_a(T_1, 5\%)/S_a$, and it is a positive value which can be greater than 1 or less than 1.

For each seismic analysis, two steps were set. The first step is a static load step, during which the gravity, hydrostatic loads, and live loads on each floor under normal operation condition were added to obtain the initial displacement and stress states for the dynamic step. The second step is a dynamic load step, wherein the earthquake wave is input, and time-history analysis is carried out. Because, under earthquake conditions, the RCF-SW of HP is more vulnerable in the stream direction, in this study, the earthquake waves were only input in the stream direction. Structural damping was incorporated using Rayleigh-type damping and a 5% damping ratio was assumed.

5. Results and Discussion

5.1. Damage Evolution. The ultimate damage state of the superstructure depends on the structural features and the input earthquake waves. However, all of the results under each record reveal a similar damage propagation process. In this section, we present the damage of the RCF-SW structure under the Koyna record.

During an earthquake, the RCF-SW structures are shaken cyclically, and the RC members will have flexure and shear behavior. When the intensity of the earthquake is large enough, the RC members will incur damage. Figure 10 shows the tensile and compressive damage profiles of the RCF-SWs under the Koyna record scaled to various intensity levels. As can be seen in Figure 10, the damage to the columns at the downstream side was more severe than that of the columns at the upstream side. The reason for this is that the auxiliary powerhouse was on the downstream side; thus, it provided support to the downstream wall, such that the stiffness changed more abruptly at the downstream column bases. Figure 11 shows the tensile and compressive damage profiles of column B (see Figure 7(d)) at the

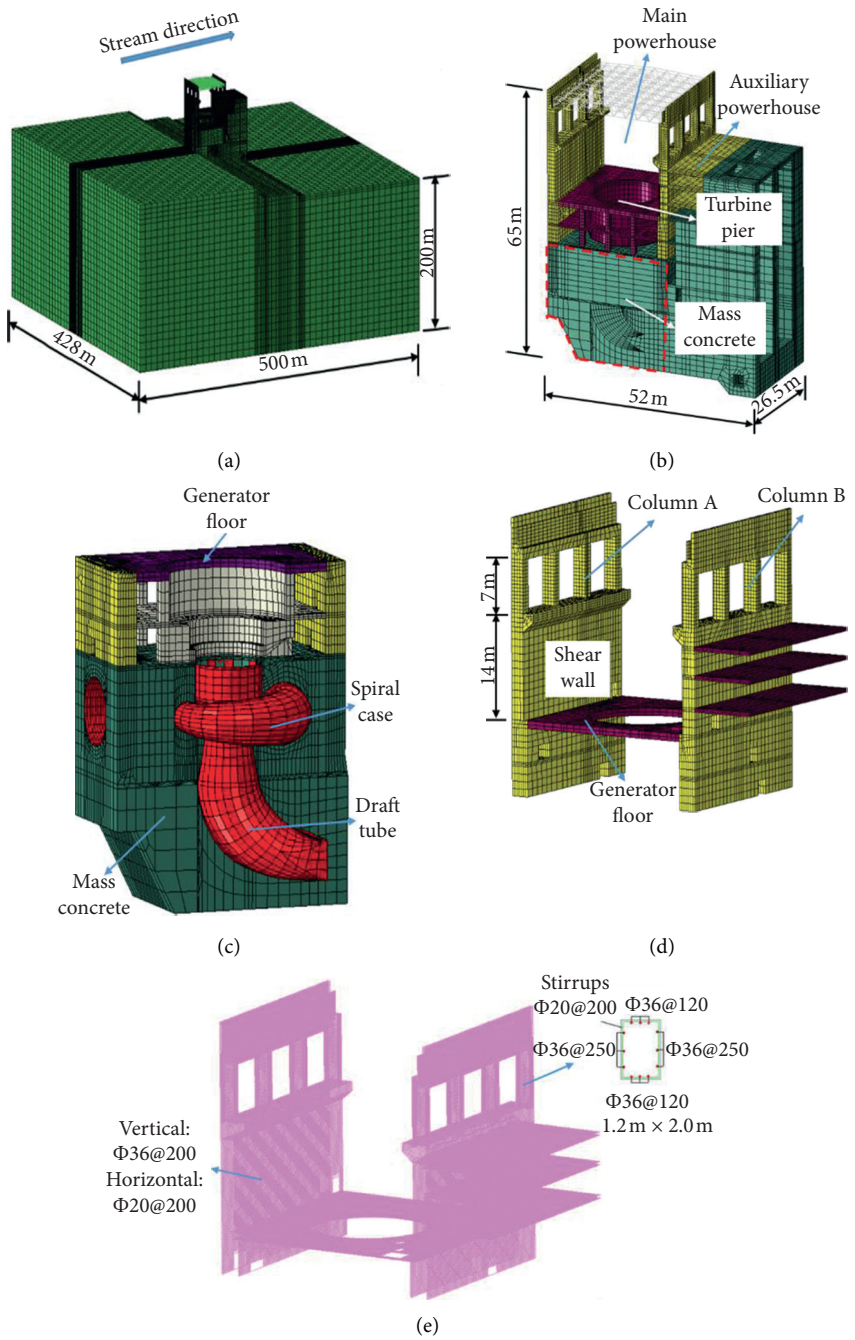

Figure 7: Geometry and FE mesh of Jx HP. (a) Global model. (b) Details of the powerhouse. (c) Substructure. (d) RCF-SW. (e) Reinforcement grids.

Table 3: Mechanical properties of materials.

Material	Young's modulus (MPa)	Poisson's ratio	Unit weight (kN/m^3)	Axial tensile strength (MPa)	Axial compressive strength (MPa)	Ultimate tensile strength (MPa)
Concrete	28,000	0.167	24	1.78	16.7	
Steel bar	200,000	0.3	78.5	400	400	540
Rock	8000	0.25	26			

downstream side. The simplified damage distribution diagrams shown in Figure 6 are in good agreement with the damage distribution profiles of column B.

The tensile damage shown in Figure 11 is larger than 0.7; therefore, the damage profiles show the possible cracking zones. Because the section size changes sharply at the column

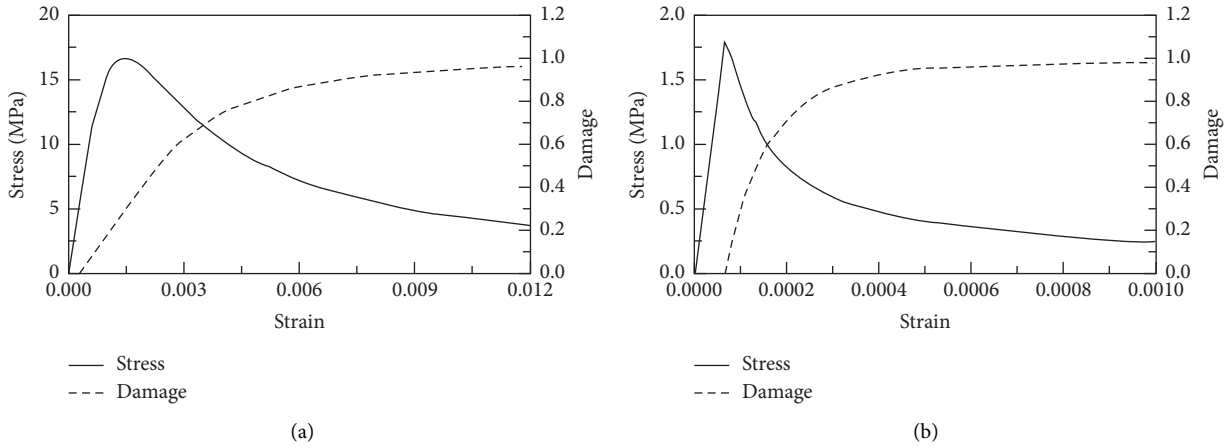

Figure 8: Uniaxial stress-strain and damage-strain curves of concrete. (a) Compression and (b) tension.

Table 4: Earthquake ground motions used in the IDA.

Number (g)	Earthquake	Year	Station	Magnitude	Rjb (km)	Rrup (km)	PGA (g)	Sa (5%) at $T_1 = 0.620$ s
1	Kobe (Japan)	1995	Kakogawa (CUE90)	6.9	22.5	22.5	0.3447	0.431
2	Chi-Chi (Taiwan)	1999	TCU045	7.62	26	26	0.361	0.404
3	Friuli (Italy)	1976	Tolmezzo (000)	6.5	14.97	15.82	0.360	0.335
4	Imperial Valley (USA)	1979	El Centro Array #2	6.53	17.32	18.81	0.3152	0.616
5	Imperial Valley (USA)	1979	El Centro Array #9	6.53	0.56	0.56	0.212	0.511
6	Loma Prieta (USA)	1989	Emeryville	6.93	76.87	76.97	0.2498	0.5978
7	Loma Prieta (USA)	1989	Gilroy Array #3	6.93	12.23	12.82	0.3674	0.425
8	Trinidad (USA)	1983	Rio Dell Overpass_ E	5.7	68.02	68.58	0.1936	0.1253
9	Northridge (USA)	1994	Castaic-Old Ridge Route	6.69	20.11	20.72	0.5683	0.7939
10	Koyna (India)	1967	IIKD006	6.3			0.464	0.372

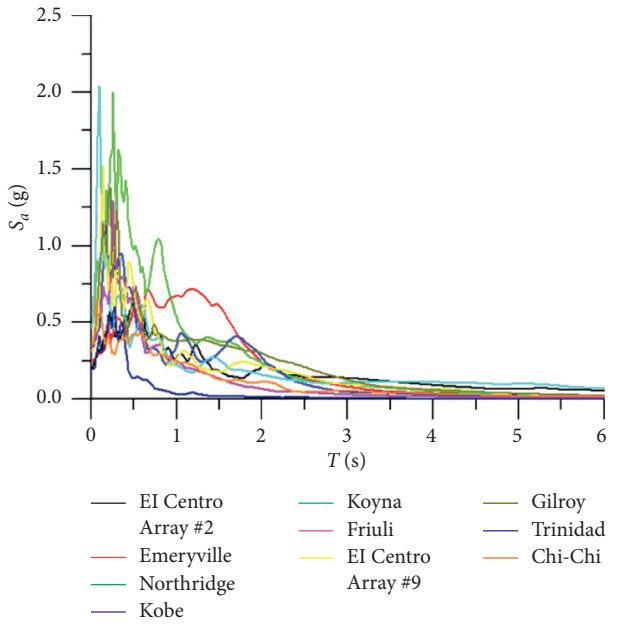

Figure 9: Acceleration response spectrum curves of all earthquake records used in the IDA.

base, the cracking initiates at the column base when $S_a(T_1, 5\%)$ is equal to 0.05 g. The cracks develop rapidly as $S_a(T_1, 5\%)$ increases. When $S_a(T_1, 5\%)$ is greater than 0.5 g, the concrete in approximately half the height of the column cracks and new cracks appear at the connection areas of the walls and floors. When $S_a(T_1, 5\%)$ reaches 1.0 g, the RCF-SWs become severely damaged. The columns are completely damaged and a crack penetrates the bottom of the upstream wall.

Additionally, the compressive damage initiates at the column base at $S_a(T_1, 5\%) = 0.2$ g and reduces from the column surface to the core. Moreover, there is no complete compressive damage, even at $S_a(T_1, 5\%) = 1.0$ g. The maximum compressive damage of the concrete cover does not exceed 0.6, and the maximum damage of the concrete core does not exceed 0.1 at $S_a(T_1, 5\%) = 1.0$ g. Increasing the shaking intensity may result in concrete crushing; however, the vastness and diffusion of the tensile damage are so significant that an accurate interpretation of the results is not possible.

As can be seen, the main damage modes of the HP are the cracking, spalling, and crushing of the columns and walls. Owing to the plastic-damage model of concrete, we can obtain the detailed damage states of the RC members and predict the engineering limit states conveniently.

5.2. IDA Results for All Records. In this section, the IDA results of the RCF-SW structure under all records are present. Figure 12 shows the IDA curves for the EDPs of individual records and their mean, median, and 16%, and 84% fractiles. Ideally, an IDA illustrates the responses of the structure by each ground motion record scaled to multiple

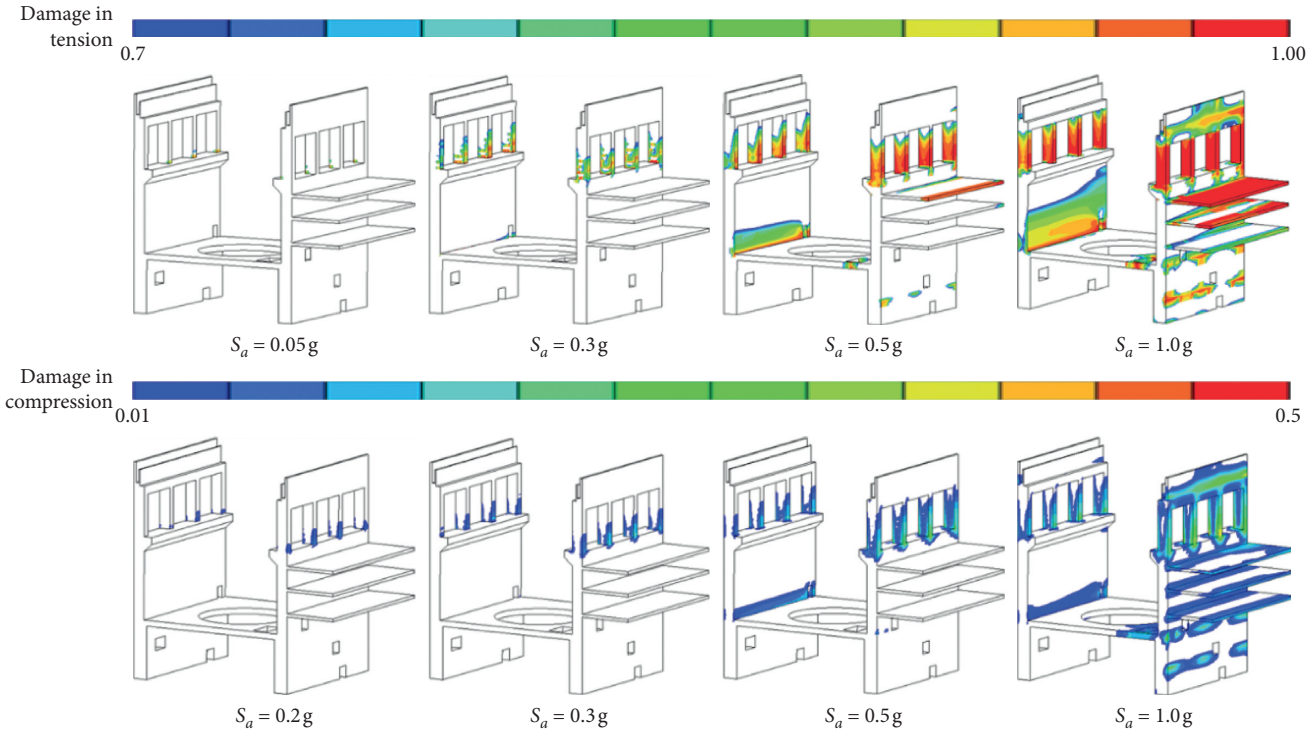

Figure 10: Ultimate damage profiles of RCF-SW structure under Koyna record.

intensities. Thus, it is possible to define the capacity and limit states of the structure, including the failure modes. However, for RC structures, the material damage induces non-convergence problems when the intensity of the record is increased to a certain value. Nevertheless, this numerical instability indicates the dynamic instability from one aspect. In this study, when $S_a(T_1, 5\%)$ exceeded 1.0 g, the tensile damage was so severe that convergence and accuracy could not be ensured simultaneously. Thus, all of the IDA curves were plotted until $S_a(T_1, 5\%) = 1.0$ g. At the point of $S_a(T_1, 5\%) = 1.0$ g, the PGA of the record varied from 0.7 g to 1.6 g. Moreover, the intensities of all records were sufficiently large, considering that the PGA at the station site with an exceedance probability of 1% per 100 years is 0.498 g.

As can be seen, the curves under different records exhibited a similar trend. However, large variation existed between the different records, particularly at high-intensity levels. When the crack penetrated the column base and the reinforcement yielded, the variations of the d/h ratio and the reinforcement stress curves became small. The mean and median curves are in better agreement at low-intensity levels, which means that the response values are distributed more evenly at low intensity. At high-intensity levels, the results were scattered by the different damage processes under various earthquake conditions.

Figure 13 shows the mean IDA curves of the EDPs based on the material damage. As shown in Figure 13, cracking initiated at the column base even at very low-intensity levels. After $S_a(T_1, 5\%) = 0.1$ g, the crack extended rapidly. Up to $S_a(T_1, 5\%) = 0.3$ g, the crack penetrated the column base under all records. The plastic hinge formed and developed from $S_a(T_1, 5\%) = 0.3$ g onwards. When $S_a(T_1, 5\%) \leq 0.05$ g, there was no compressive damage for most records. The average compressive damage of the column cover $D_{\text{c-cover}}$ ranged from 0 to 0.55. The spalling of the concrete cover started at approximately $S_a(T_1, 5\%) = 0.3$ g on average and reached up to $S_a(T_1, 5\%) = 1.0$ g; severe spalling appeared only under three records. The compressive damage of the concrete core was slighter than that of the concrete cover. The average compressive damage of the column core $D_{\text{c-core}}$ ranged from 0 to 0.3. The crushing of the concrete core started at approximately $S_a(T_1, 5\%) = 0.55$ g, on average, and reached up to $S_a(T_1, 5\%) = 1.0$ g; none of the results indicates severe crushing.

The reinforcement stresses were mainly affected by the tensile damage. From $S_a(T_1, 5\%) = 0.05$ g onwards, the reinforcement stresses began to increase rapidly. After $S_a(T_1, 5\%) = 0.3$ g, the stress values of various records became obviously scattered. At this point, the concrete damage entered the quick developing stage, and the variation between the different records became larger. The yielding of the reinforcement began at $S_a(T_1, 5\%) = 0.7$ g, on average. After $S_a(T_1, 5\%) = 0.9$ g, the reinforcement yielded under all earthquake records.

5.3. Damage State Prediction Based on Material Damage. According to the list of EDP limitations in Table 2, we can distinguish the engineering limit states and predict the damage states of the RC members. Table 5 lists the engineering limit states, damage states, and corresponding $S_a(T_1, 5\%)$. By using different EDPs, the damage state

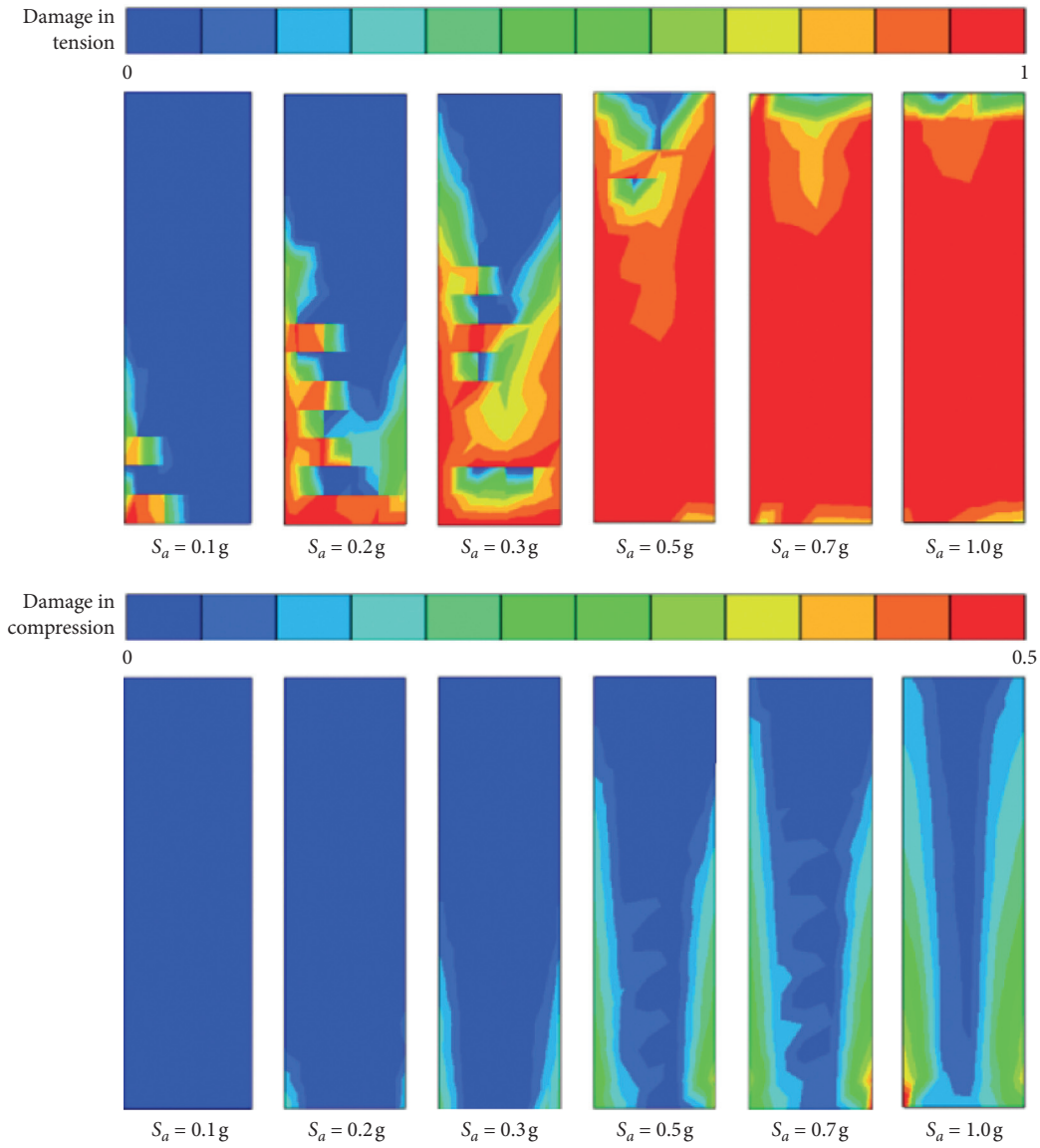

Figure 11: Ultimate damage profiles of column B under Koyna record.

division points vary. For example, D_{c-core} predicts the moderate damage state at $S_a(T_1, 5\%) = 0.59\,g$ and the reinforcement stress at $S_a(T_1, 5\%) = 0.65\,g$. However, the two division points are close to each other. By considering all of the engineering limit states, we can summarize this as follows: $S_a(T_1, 5\%) = 0.1\,g$ is considered as a negligible damage state; $S_a(T_1, 5\%) = 0.35\,g$ is considered as a light damage state; $S_a(T_1, 5\%) = 0.6\,g$ is considered as a moderate damage state.

The results revealed that the RCF-SW structure of the HP had good aseismic capacity. Severe spalling, critical crushing, and collapse were not observed, even after scaling $S_a(T_1, 5\%)$ up to 1.0 g. This means that the RC frame and shear wall incurred only moderate damage, even under rare earthquakes. The damage state prediction is in agreement with the design principle of hydraulic structures. The seismic-resistant objectives for hydraulic structures should be higher than those of ordinary buildings, considering the importance of hydraulic structures. In practice, hydraulic structures are designed to ensure that damage does not occur under minor earthquakes, repairable damage occurs under moderate earthquakes, and collapse does not occur under strong earthquakes.

5.4. Comparison of Damage State Prediction Based on Drift Ratio and Material Damage. Drift ratio is widely used in the seismic performance assessment of RC columns and walls. The drift ratio limitations that have been commonly used in related studies [4, 31–33] for each damage state are listed in Table 6. Employing the drift ratio as an EDP, the damage states are assessed, as shown in Figures 14 and 15.

Even though the concrete damage appeared at a very low-intensity level, the drift curves exhibited linear behavior approximately up to $S_a(T_1, 5\%) = 0.6\,g$. When

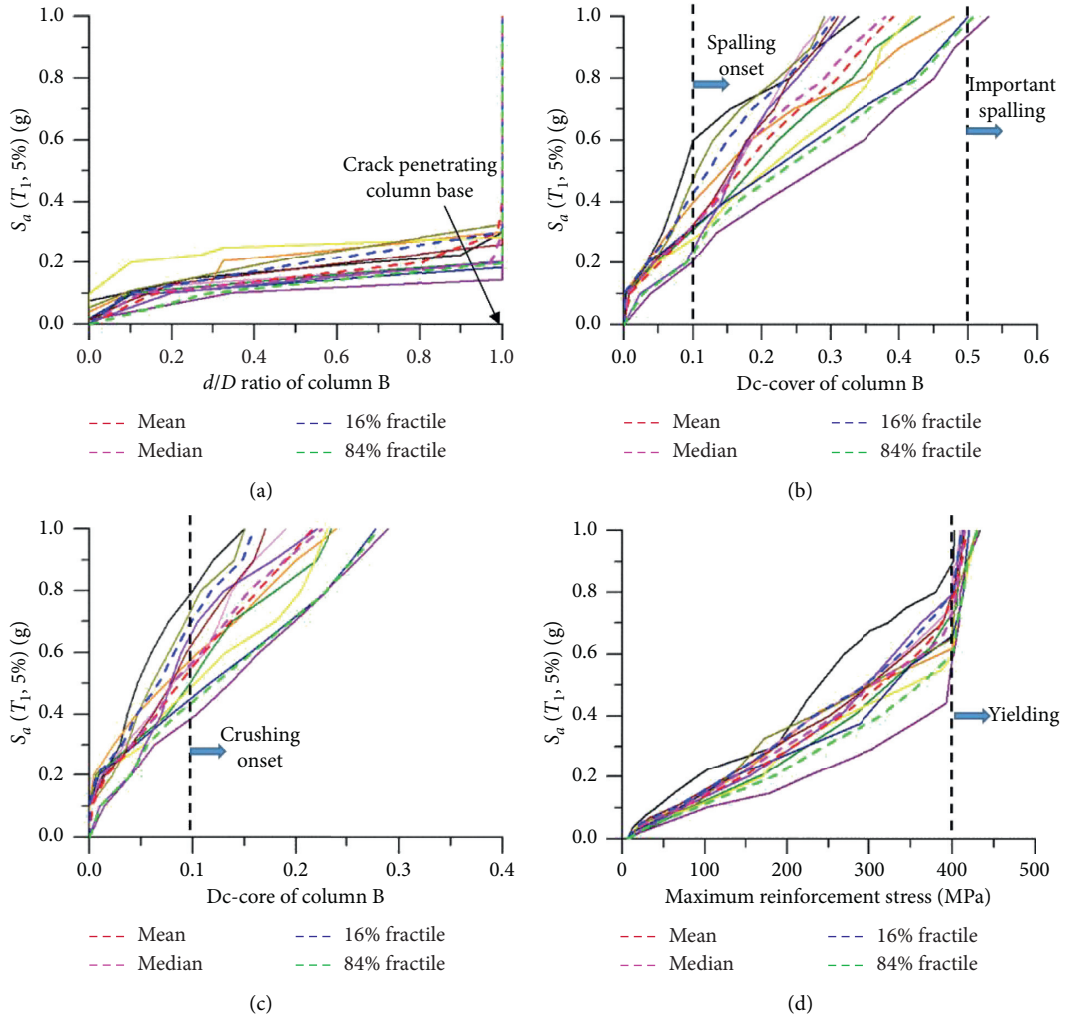

Figure 12: IDA curves of EDPs. (a) d/h. (b) $D_{c-cover}$ of column B. (c) D_{c-core} of column B. (d) Reinforcement stress.

$S_a(T_1, 5\%) < 0.6$ g, the tensile damage was severe, but the compressive damage was still at the early developing stage. This means that the tensile damage does not significantly influence the deformation of the RC frame, although the compressive damage does. Despite the severe damage at $S_a(T_1, 5\%) = 1.0$ g, the maximum drift ratios of the columns and walls during the earthquake did not exceed 0.8%. The damage limit states revealed by the column drift ratios are approximately the same as those revealed by the drift ratio of the shear wall. Using the drift ratio index, $S_a(T_1, 5\%) = 0.3$ g can be regarded as a negligible damage state, $S_a(T_1, 5\%) = 0.6$ g can be regarded as a light damage state, and $S_a(T_1, 5\%) = 0.9$ g can be regarded as a moderate damage state. These results are quite different from those obtained by the material damage EDPs.

When $S_a(T_1, 5\%)$ reached 0.3 g, the structural damage was regarded as negligible by using the limitation of the 1/550 elastic drift ratio. However, at this point, the column base had already been penetrated by the cracks, and the concrete was almost completely damaged from the column base to the half-height of the column. Additionally, the concrete cover at the column base became spalled. From the viewpoint of material damage and RC members, this damage cannot be ignored. When $S_a(T_1, 5\%)$ reached 0.6 g, the crushing of the concrete cover and the yielding of the reinforcement were observed. This indicates that the cohesiveness between the concrete and the reinforcement was damaged and that a plastic region formed at the column base. The deformation of the structure increased faster when the earthquake intensity was increased further. Therefore, the columns should be rehabilitated before use. The damage at $S_a(T_1, 5\%) = 0.6$ g was regarded as moderate by using the material damage EDPs. However, a light damage state was recognized by the drift ratio index.

Generally, the drift ratio represents the damage states of regular buildings at a global level, and the determination of the elastic and plastic drift ratio limitations is based on the investigation of ordinary RC members and frames. Additionally, the story displacement differential causing the structural damage is the story displacement differential in the direction parallel to the floors. However, the drift ratios are approximated using the horizontal displacement of the vertical members, but this calculation method introduces error. Particularly, for HPs, because of the huge sectional

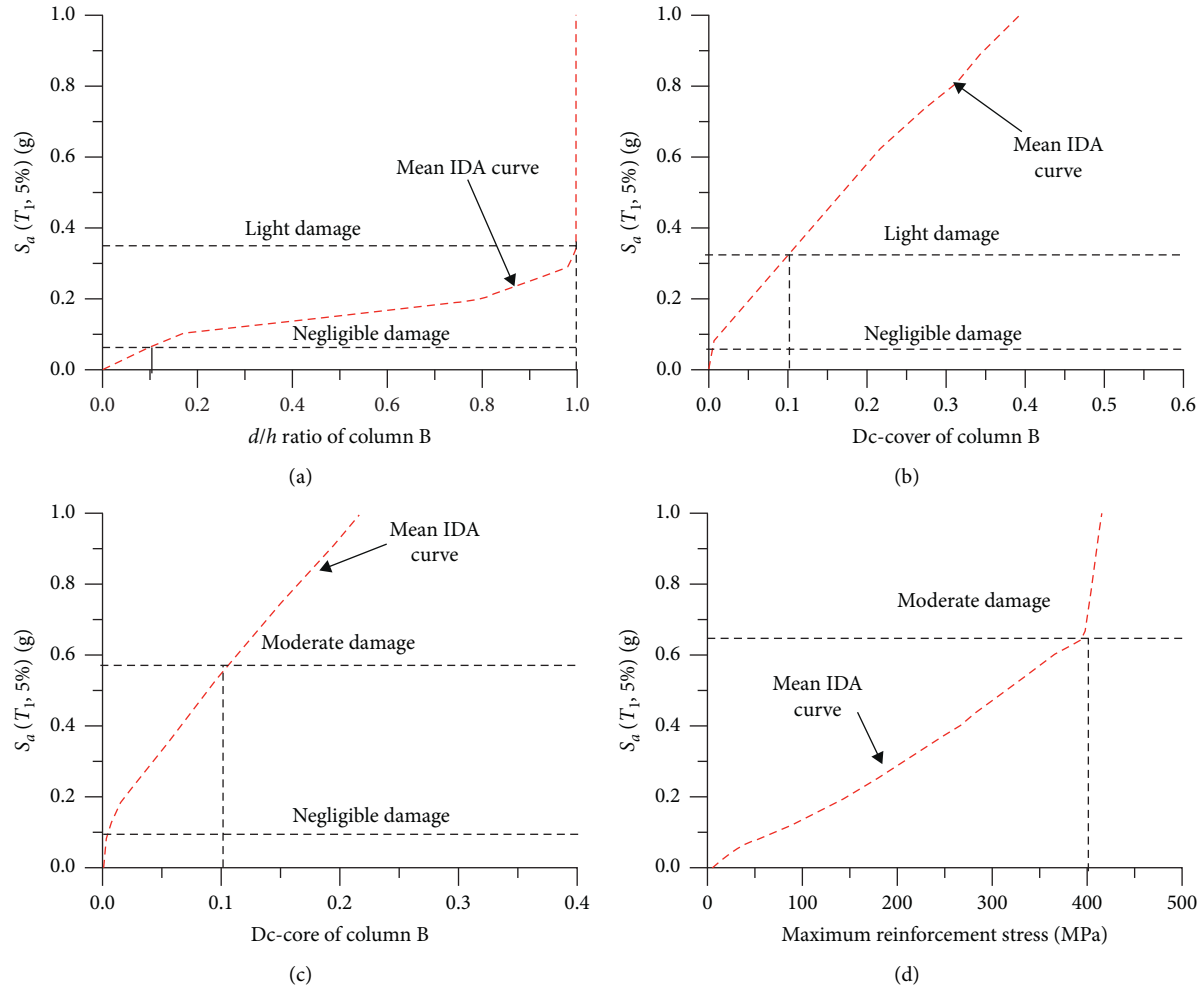

Figure 13: Mean IDA curves of EDPs. (a) d/h. (b) $D_{c-cover}$ of column B. (c) D_{c-core} of column B. (d) Reinforcement stress.

Table 5: Engineering limit state and damage state prediction.

$S_a(T_1, 5\%)$ (g)	EDP	Engineering limit state	Damage state
0.08	$d/h = 0.1$	Concrete cover cracking onset	Negligible
0.10	$D_{c-cover} \approx 0$; $D_{c-core} \approx 0$	No or slight compressive damage	Negligible
0.32	$D_{c-cover} = 0.1$	Concrete cover spalling onset	Light
0.36	$d/h = 1$	Plastic hinge initiating	Light
0.59	$D_{c-core} = 0.1$	Concrete core crushing onset	Moderate
0.65	$\sigma_s = \sigma_y$	Steel bar yielding	Moderate

Table 6: Drift ratio limitations for column and wall at different damage states.

Element	Damage state			
	Negligible	Light	Moderate	Severe
Column	1/550	1/275	1/140	1/50
Wall	1/1000	1/500	1/250	1/120

sizes, large reinforcement ratio, support of auxiliary powerhouse at the downstream side, and link provided by the roof grids, the drift ratios of the RC columns and shear walls are not large. Even at $S_a(T_1, 5\%) = 1.0$ g, the maximum drift ratio did not exceed 1%. Therefore, the material damage states of the RC members in the HP are not always consistent with the damage states identified by the drift ratio. For a structure whose damage is controlled by the members, the drift ratio is not always suitable.

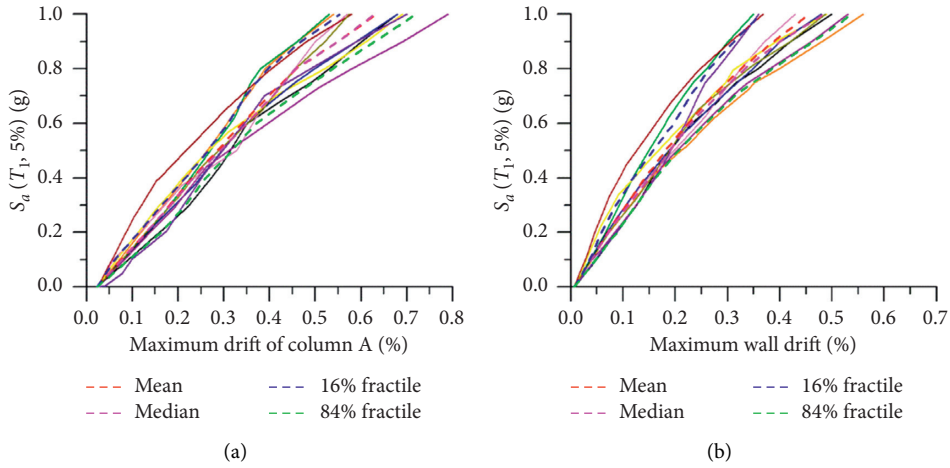

Figure 14: IDA curves of drift ratio. (a) Column A and (b) wall.

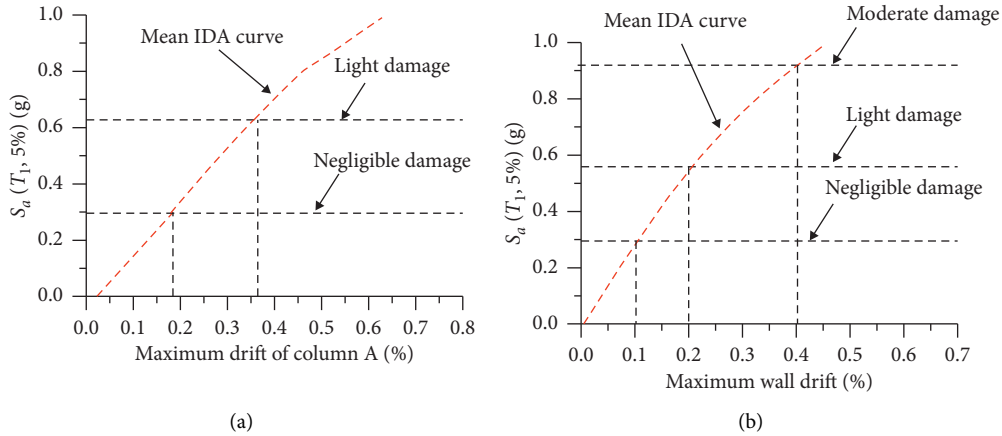

Figure 15: Mean IDA curves of drift ratio. (a) Column A and (b) wall.

6. Conclusions

In this study, the seismic performance of an RCF-SW structure in an HP was investigated by IDA employing a plastic-damage concrete model. Several EDPs based on material damage are proposed to track the damage extent to the structure. These EDPs associated with the mean IDA curves are suggested to identify the engineering limit states and damage levels of RCF-SW structures at the member level. By considering an HP in China as a case study, a large-scale FE model was developed, and IDAs were performed on ten records. Thus, the following conclusions were drawn.

The main damage mode of the RCF-SW structure in the HP was the damage of the RC members. Generally, the RCF-SW structure incurred the cracking of the columns and walls and the crushing of the columns. The EDPs based on material damage revealed the material damage evolution of the RC members and easily distinguished the engineering limit states, such as cracking, crushing, reinforcement yielding, and plastic hinge forming. These engineering limit states were used to identify the damage state of the RC members. Therefore, a relationship between the EDPs and damage states was established. IDA and concrete damage mechanism were powerful tools to predict the damage states of RCF-SW structures in HPs. The EDPs based on material damage could be used to evaluate the seismic performance of RCR-SW structures as other indices, such as the peak drift ratios residual drift ratio, stiffness degradation, and dissipated energy.

The mean IDA curves of the drift ratio exhibited a linear trend that ended at the beginning point of the crushing of the concrete core and the yielding of reinforcement. The damage states identified by the drift ratio were lighter than those identified by the EDPs based on material damage. For an RCF-SW structure whose damage was controlled by the members, it is more suitable to use the EDPs based on material damage to identify the damage states, instead of using the drift ratio. Additionally, the EDPs based on material damage were linked to engineering limit states; thus, this may provide useful information for the aseismic

measure determination and postquake rehabilitation of RC members.

Data Availability

The earthquake ground motion data used to support the findings of this study are available on https://peer.berkeley.edu/peer-strong-ground-motion-databases.

Conflicts of Interest

The authors declare that there are no conflicts of interest regarding the publication of this paper.

Acknowledgments

This study was financially supported by the National Natural Science Foundation of China (nos. 51679175, 51679013, and 51609020).

References

[1] J. P. Moehle, "Displacement-based design of RC structures subjected to earthquakes," *Earthquake Spectra*, vol. 8, no. 3, pp. 403–428, 1992.

[2] Structural Engineers Association of California (SEAOC), "Performance based seismic engineering of buildings," SEAOC, Sacramento, CA, USA, SEAOC Vision 2000, 1995.

[3] Federal Emergency Management Agency (FEMA), "Next generation performance-based design guidelines," FEMA, Washington, DC, USA, FEMA-445, 2006.

[4] Federal Emergency Management Agency (FEMA), "NEHRP guidelines for the seismic rehabilitation of buildings," FEMA, Washington, DC, USA, FEMA-273, 1997.

[5] Federal Emergency Management Agency (FEMA), "Pre-standard and commentary for the seismic rehabilitation of buildings," FEMA, Washington, DC, USA, FEMA-356, 2000.

[6] Applied technology council (ATC), "Seismic evaluation and retrofit of concrete buildings," ATC, CA, USA, ATC-40, 1996.

[7] M. Alembagheri, "Earthquake damage estimation of concrete gravity dams using linear analysis and empirical failure criteria," *Soil Dynamics and Earthquake Engineering*, vol. 90, pp. 327–339, 2016.

[8] M. Alembagheri and M. Ghaemian, "Damage assessment of a concrete arch dam through nonlinear incremental dynamic analysis," *Soil Dynamics and Earthquake Engineering*, vol. 44, no. 1, pp. 127–137, 2013.

[9] M. Alembagheri and M. Ghaemian, "Seismic assessment of concrete gravity dams using capacity estimation and damage indexes," *Earthquake Engineering & Structural Dynamics*, vol. 42, no. 1, pp. 123–144, 2013.

[10] M. Alembagheri and M. Ghaemian, "Seismic performance evaluation of a jointed arch dam," *Structure and Infrastructure Engineering*, vol. 12, no. 2, pp. 256–274, 2016.

[11] A. Amirpour and H. Mirzabozorg, "Quantifying the qualitative limit-states using IDA approach in concrete arch dams," *Arabian Journal for Science and Engineering*, vol. 39, no. 11, pp. 7729–7740, 2014.

[12] H. Q. Chen, D. Y. Li, and S. S. Guo, "Damage-rupture process of concrete dams under strong earthquakes," *International Journal of Structural Stability & Dynamics*, vol. 14, no. 7, Article ID 1450021, 2014.

[13] C. H. He, J. T. Wang, and C. H. Zhang, "Determination of seismic parameters for dam sites by numerical simulation of the rupture-canyon wave field," *Chinese Journal of Geophysics*, vol. 60, no. 2, pp. 585–592, 2017.

[14] Z. Y. Yang, B. Wang, and J. P. Zhou, *Seismic Damage Investigation on Large and Medium Sized Hydropower Projects in Wenchuan Earthquake Area*, Water & Power Press, Beijing, China, 2009.

[15] L. J. Zhang, H. Y. Zhang, Y. X. Ji et al., "Whiplash effect on hydropower house during an earthquake," *International Journal of Structural Stability & Dynamics*, vol. 14, no. 4, Article ID 1450007, 2014.

[16] J. G. Hao, L. Hu, H. G. Wu et al., "Failure modes of hydropower house superstructure under rare earthquake action," *Journal of Vibration and Shock*, vol. 35, no. 3, pp. 55–61, 2016.

[17] China Renewable Energy Engineering Institute, "Design specification for powerhouses of hydropower stations," China Renewable Energy Engineering Institute, Beijing, China, NB/T-35011-2013, 2013.

[18] US Army Corps of Engineers (USACE), "Earthquake design and evaluation of concrete hydraulic structures," USACE, Washington, DC, USA, EM-1110-2-6053, 2007.

[19] D. Vamvatsikos and C. A. Cornell, "Incremental dynamic analysis," *Earthquake Engineering & Structural Dynamics*, vol. 31, no. 3, pp. 491–514, 2002.

[20] E. Brunesi, R. Nascimbene, F. Parisi, and N. Augenti, "Progressive collapse fragility of reinforced concrete framed structures through incremental dynamic analysis," *Engineering Structures*, vol. 104, pp. 65–79, 2015.

[21] D. Vamvatsikos and M. Fragiadakis, "Incremental dynamic analysis for estimating seismic performance sensitivity and uncertainty," *Earthquake Engineering & Structural Dynamics*, vol. 39, no. 2, pp. 141–163, 2010.

[22] W. P. Wu, L. F. Li, L. H. Wu et al., "Evaluation of seismic vulnerability of high-pier long-span bridge using incremental dynamic analysis," *Journal of Earthquake Engineering and Engineering Vibration*, vol. 32, no. 3, pp. 117–123, 2012.

[23] A. Ghobarah, "On drift limits associated with different damage levels," in *Proceedings of the International Workshop on Performance-Based Seismic Design Concepts and Implementation*, Bled, Slovenia, June 2004.

[24] Y. J. Park and A. H. S. Ang, "Mechanistic seismic damage model for reinforced concrete," *Journal of Structural Engineering*, vol. 111, no. 4, pp. 722–739, 1985.

[25] G. H. Powell and R. Allahabadi, "Seismic damage prediction by deterministic methods: concepts and procedures," *Earthquake Engineering & Structural Dynamics*, vol. 16, no. 5, pp. 719–734, 1988.

[26] H. Horii and S.-C. Chen, "Computational fracture analysis of concrete gravity dams by crack-embedded elements-toward an engineering evaluation of seismic safety," *Engineering Fracture Mechanics*, vol. 70, no. 7-8, pp. 1029–1045, 2003.

[27] Y. Calayir and M. Karaton, "A continuum damage concrete model for earthquake analysis of concrete gravity dam-reservoir systems," *Soil Dynamics and Earthquake Engineering*, vol. 25, no. 11, pp. 857–869, 2005.

[28] K. Kunnath, E. Sashi, Bahy et al., "Cumulative seismic damage of reinforced concrete bridge piers," NCEER Report: 97-0006, National Center for Earthquake Engineering Research, State University of New York at Buffalo, New York, NY, USA, 1997.

[29] D. Lehman, J. Moehle, S. Mahin, A. Calderone, and L. Henry, "Experimental evaluation of the seismic performance of

reinforced concrete bridge columns," *Journal of Structural Engineering*, vol. 130, no. 6, pp. 869–879, 2004.

[30] T.-H. Kim, K.-M. Lee, Y.-S. Chung, and H. M. Shin, "Seismic damage assessment of reinforced concrete bridge columns," *Engineering Structures*, vol. 27, no. 4, pp. 576–592, 2005.

[31] A. Belejo, A. R. Barbosa, and R. Bento, "Influence of ground motion duration on damage index-based fragility assessment of a plan-asymmetric non-ductile reinforced concrete building," *Engineering Structures*, vol. 151, pp. 682–703, 2017.

[32] Ministry of Construction of the People's Republic of China, "Code for seismic design of buildings," Ministry of Construction of the People's Republic of China, Beijing, China, GB50011-2010, 2010.

[33] K. G. Smith, "Innovation in earthquake resistant concrete structure design philosophies; a century of progress since Hennebique's patent," *Engineering Structures*, vol. 23, no. 1, pp. 72–81, 2001.

[34] L. Xin, W. Liang, and L. Bai, "Optimal method for direct displacement-based seismic design of RC frames," *Journal of Earthquake Engineering & Engineering Vibration*, vol. 28, no. 5, pp. 79–86, 2008.

[35] A. Ghobarah, H. Abou-Elfath, and A. Biddah, "Response-based damage assessment of structures," *Earthquake Engineering & Structural Dynamics*, vol. 28, no. 1, pp. 79–104, 1999.

[36] J. Hancock and J. J. Bommer, "A state of knowledge review of the influence of strong-motion duration on structural damage," *Earthquake Spectra*, vol. 22, no. 3, pp. 827–845, 2006.

[37] R. Chandramohan, J. W. Baker, and G. G. Deierlein, "Quantifying the influence of ground motion duration on structural collapse capacity using spectrally equivalent records," *Earthquake Spectra*, vol. 32, no. 2, pp. 927–950, 2016.

[38] J. Lee and G. L. Fenves, "A plastic-damage concrete model for earthquake analysis of dams," *Earthquake Engineering & Structural Dynamics*, vol. 27, no. 9, pp. 937–956, 1998.

[39] O. Omidi, S. Valliappan, and V. Lotfi, "Seismic cracking of concrete gravity dams by plastic-damage model using different damping mechanisms," *Finite Elements in Analysis and Design*, vol. 63, no. 1, pp. 80–97, 2013.

[40] Y. Yazdani and M. Alembagheri, "Seismic vulnerability of gravity dams in near-fault areas," *Soil Dynamics and Earthquake Engineering*, vol. 102, pp. 15–24, 2017.

[41] Y. A. Heo, *Framework for damage-based probabilistic seismic performance evaluation of reinforced concrete frames*, Ph.D. thesis, University of California Davis, Davis, CA, USA, 2009.

[42] Z. X. Li, Y. Chen, and N. Li, "A damage model for reinforced concrete members based on material damage," *Engineering Mechanics*, vol. 31, no. 6, pp. 53–59, 2014.

[43] X. J. Du, "Methodology research on seismic performance assessment based on damage for RC frame structures," Master thesis, Huazhong University of Science and Technology, Wuhan, China, 2015.

[44] ABAQUS Inc, *ABAQUS Theory Manual (Version 6.6)*, Dassault Systèmes Americas, Waltham, MA, USA, 2006.

[45] J. Lee and G. L. Fenves, "Plastic-damage model for cyclic loading of concrete structures," *Journal of Engineering Mechanics*, vol. 124, no. 8, pp. 892–900, 1998.

[46] China State Bureau of Quality and Technical Supervision, "Code for design of concrete structures," China Architecture & Building Press, Beijing, China, GB 50010-2010, 2015.

[47] F. Lgeron and P. Paultre, "Behavior of high-strength concrete column under cyclic flexure and constant axial load," *ACI Structural Journal*, vol. 97, no. 4, pp. 591–601, 2000.

[48] L. I. Cardona, P. Paultre, and J. Mazars, "Damage mechanics applied to performance-based design of reinforced concrete columns," *Earthquake Engineering & Structural Dynamics*, vol. 46, no. 3, pp. 2439–2457, 2017.

[49] J. H. Ouyang, H. Q. Chen, C. R. Zhang et al., "Dynamic response analysis on no. 15 unit powerhouse structure in the Three Gorges hydropower station," *Journal of China Institute of Water Resources & Hydropower Research*, vol. 5, no. 2, pp. 137–142, 2007.